Original Article

Structural and mechanistic studies of γ-Fe_2O_3 nanoparticle as troxacitabine drug nanocarrier

Neda Mozayyeni, Ali Morsali*, Mohammad R. Bozorgmehr, S. Ali Beyramabadi

Department of Chemistry, Mashhad Branch, Islamic Azad University, Mashhad, Iran & Research Center for Animal Development Applied Biology, Mashhad Branch, Islamic Azad University, Mashhad 917568, Iran.

Abstract

Using density functional theory, noncovalent interactions and three mechanisms of covalent functionalization of troxacitabine anticancer drug onto γ-Fe_2O_3 nanoparticles have been investigated. Quantum molecular descriptors of noncovalent configurations were studied. It was specified that binding of troxacitabine onto γ-Fe_2O_3 nanoparticles is thermodynamically suitable. Hardness and the gap of energy between LUMO and HOMO of troxacitabine are higher than the noncovalent configurations, showing the reactivity of troxacitabine increases in the presence of γ-Fe_2O_3 nanoparticles. Troxacitabine can bond to γ-Fe_2O_3 nanoparticles through NH_2 (k_1 mechanism), OH (k_2 mechanism) and CO (k_3 mechanism) groups. The activation energies, the activation enthalpies and the activation Gibbs free energies of these reactions were calculated. It was specified that the k_1 and k_2 mechanisms are under thermodynamic control and the k_3 mechanisms is under kinetic control. These results could be generalized to other similar drugs.

Keywords: γ-Fe_2O_3 nanoparticles, troxacitabine, density functional theory, noncovalent and covalent functionalization, mechanism

Introduction

One of the nanoscale materials being extensively utilized are magnetic nanoparticles (MNPs) [1-4]. MNPs are made of elements such as iron, nickel, cobalt, and their oxides, and many of their applications are related to iron oxide nanoparticle. MNPs show unique magnetic, electronic, and chemical properties, causing them to be used for biological and pharmaceutical researches [5-10]. The large surface to volume ratio provides the possibility of functionalization of different molecules, including the therapeutic agents, to them [11-14].

Although many efforts have been made to overcome cancer through chemotherapy, but unfortunately, the old strategies and approaches produce many side effects such as vomiting, hair loss, cardio-toxicity and breathing troubles in the patients. The higher the dose of anti-cancer drugs prescribed and used, the higher the increase of toxicity in the tissues and immune system of the body [15, 16].

The magnetic properties of MNPs cause them to have numerous applications in connection with the drug delivery and diagnostics and therapeutics. The drug delivery systems, using MNPs as carrier, have been based on the fact that they could be guided to a specific location such as a cancerous tumor by using external magnetic field [17, 18]. After arrival of MNPs at the target site, the drug is released through the enzymatic activity or through changes in pH, temperature, and osmolality [19, 20].

Iron oxide could exist along with different chemical compositions, such as magnetite (Fe_3O_4) and maghemite (γ-Fe_2O_3). Magnetite and maghemite have the utmost usage in biomedical applications. Covalent and noncovalent (hydrogen bonds and van der Waals interactions) functionalizations play a principle role in the drug delivery systems. The possibility of targeted drug delivery causes reduction of the amount of drugs consumed and consequently the reduction of their side effects [21-23].

Troxacitabine or 4-amino-1-[(2S)-2-(hydroxymethyl)-1,3-dioxolan-4-yl]pyrimidin-2-one (TC) is a synthetic L-nucleoside analogue which has antitumor and anticancer activities and is highly effective in the treatment of advanced leukemia [24, 25].

For the development of drug delivery systems by using MNPs, it is necessary to present molecular models for understanding the mechanism of functionalization of the drugs to these nanoparticles in solvents (especially water). Quantum calculations could be of great assistance to the design and analysis of drug delivery systems. The granting of Nobel Prize for chemistry in 2016 for the design and manufacturing of molecular machines, TCable of being used in drug deliverance as well, confirms our statement [26-28].

Address for correspondence: Ali Morsali, Department of Chemistry, Mashhad Branch, Islamic Azad University, Mashhad, Iran.
Email: almorsali@yahoo.com, morsali@mshdiau.ac.ir

How to cite this article: Mozayyeni, N., Morsali, A., Bozorgmehr, M. R., Beyramabadi, S. A. Structural and mechanistic studies of γ-Fe2O3 nanoparticle as troxacitabine drug nanocarrier. Arch Pharma Pract 2019;10(1):31-7.

We have used quantum calculations for analysis of more stable structures and the mechanism of functionalization of troxacitabine drug to γ-Fe_2O_3 nanoparticles. Such calculations could inspire researchers to manufacture new drug delivery systems. In spite of different theoretical studies on MNPs, so far, few studies have been done on the mechanism of functionalization in solution.

Computational Method

All calculations have been done with the B3LYP [29-31] hybrid density functional level using the GAUSSIAN 09 package [32]. The 6-31G(d,p) basis set was used except for Fe where the LANL2DZ basis set was employed with effective core potential (ECP) functions.

The solvent plays a key role in chemical systems explicitly [33-40] or implicitly. Polarized continuum model (PCM) was used for the consideration of implicit effects of the solvent.[41, 42]. For all species, all degrees of freedom were optimized. The transition state obtained was confirmed to have only one imaginary frequency of the Hessian. The zero-point corrections were also considered to obtain activation energy.

Results and Discussion

Noncovalent functionalization

Troxacitabine (TC) is a nonplanar molecule with NH_2, oH, CO, and F groups as presented in Fig. 1. γ-Fe_2O_3 nanoparticle was modeled using $Fe_6(OH)_{18}(H_2O)_6$ ring clusters of six-edge sharing octahedra joining via 12 OH groups [43]. The optimized geometries of γ-Fe_2O_3 nanoparticle (MNP) and troxacitabine (TC) in solution phase are presented in Fig. 1.

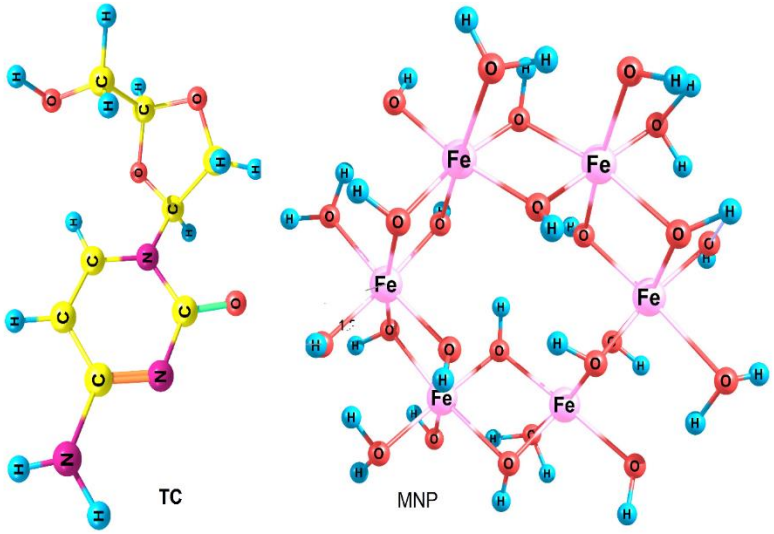

Fig. 1. Optimized structures of MNP and TC.

The interaction between TC and MNP through NH_2 (MNP/TC1), OH (MNP/TC2), and CO (MNP/TC3) groups was considered in gas and solution phases. These three configurations have been shown in Figures 2-4 (See supporting information for Cartesian coordinates of the calculated structures).

The solvation energies of TC, MNP, and MNP/TC1-3 have been shown in Table 1. The binding energies (ΔE) of TC to MNP in gas and solution phases were calculated using the following equation and presented in Table 1:

$$\Delta E = E_{MNP/TC1-3} - (E_{MNP} + E_{TC}) \qquad (1)$$

The calculated solvation energies show that TC solubility increases in the presence of MNP. The calculated binding energies of MNP/TC2 and MNP/TC2 are negative in gas and solution phases. MNP/TC3 is more stable than MNP/CAP2-3 in both phases.

Table 1. Solvation and binding energies of different configurations (kJ mol-1).

Species	Solvation energy	Binding energy	Binding energy
TC	-58.84	Solution phase	Gas phase
MNP	-126.25		
MNP/TC1	-168.78	13.89	-2.41
MNP/TC2	-158.58	-12.94	-39.45
MNP/TC3	-176.56	-37.97	-46.50

Quantum molecular descriptors such as hardness and electrophilicity index could be used to describe chemical reactivity and stability. The global hardness (η) indicates the resistance of one molecule against the change in its electronic structure (Equation 2). Decrease in η causes a decrease in the reactivity and an increase in stability.

$$\eta = (I - A)/2 \qquad (2)$$

where $I = -E_{HOMO}$ and $A = -E_{LUMO}$ are the ionization potential and the electron affinity of the molecule, respectively. Parr defined the electrophilicity index (ω) as follows [44]:

$$\omega = (I + A)^2 / 4\eta \qquad (3)$$

Table 2. Quantum molecular descriptors (eV) and binding energies (kJ mol^{-1}) of TC, MNP, and MNP/TC1-3.

Species	E_{HOMO}	E_{LUMO}	E_g	η	ω
Solution phase (water)					
TC	-6.29	-0.80	5.49	2.75	2.28
MNP	-5.58	-4.48	1.10	0.55	22.95
MNP/TC1	-5.62	-4.51	1.10	0.55	23.28
MNP/TC2	-5.63	-4.53	1.10	0.55	23.37
MNP/TC3	-5.67	-4.66	1.00	0.50	26.54
Gas phase					
TC	-6.12	-0.75	5.37	2.69	2.20
MNP	-5.41	-4.36	1.05	0.53	22.68
MNP/TC1	-5.67	-4.61	1.06	0.53	24.84
MNP/TC2	-5.56	-4.56	0.99	0.50	25.79
MNP/TC3	-5.24	-4.13	1.11	0.55	19.84

Table 2 presents the quantum molecular descriptors for TC, MNP, and MNP/TC1-4 in both phases. In this table, Eg (gap of energy between LUMO and HOMO) was also calculated. Eg notably determines a more stable configuration.

According to the data in Table 2, η and *Eg* related to the TC drug are higher than those of MNP/TC1-3, showing the reactivity of TC increases in the presence of MNP. ω of TC increases in the presence of MNP, showing that TC acts as electron acceptor.

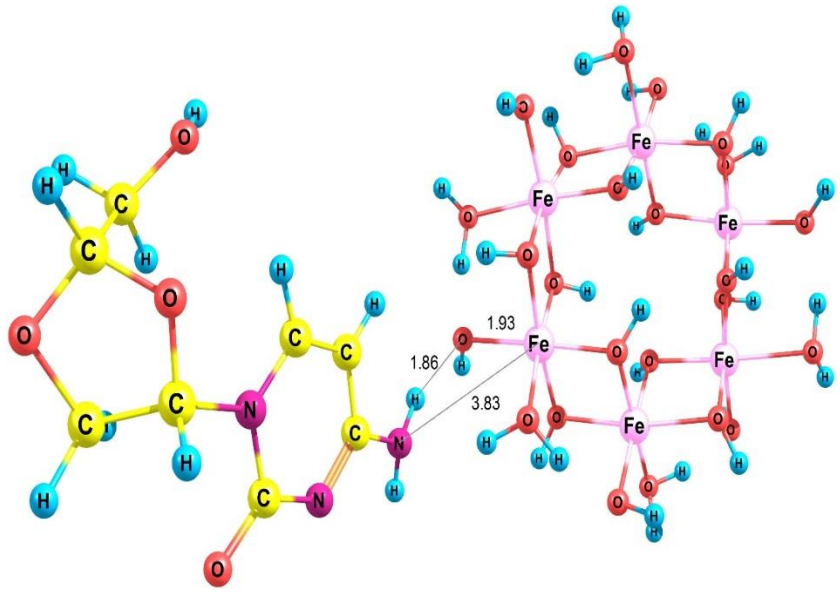

Fig. 2. Optimized structure of MNP/TC1.

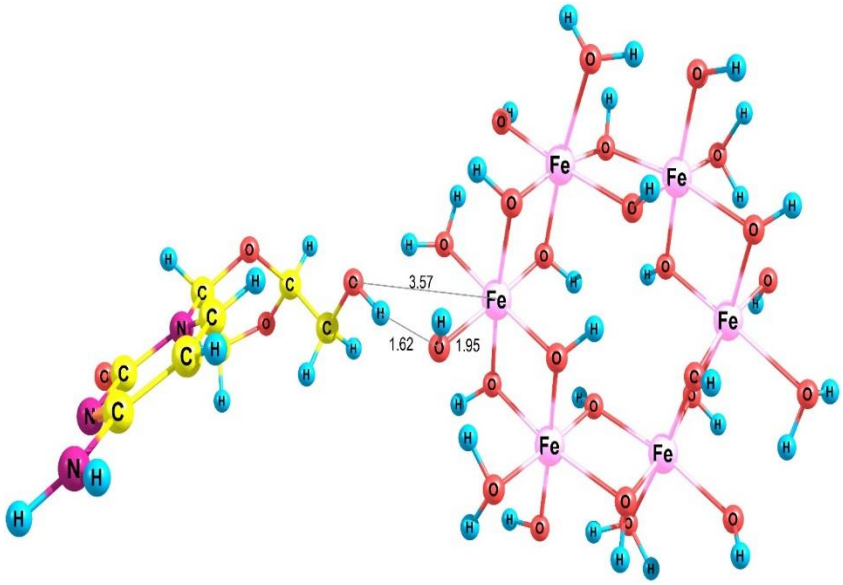

Fig. 3. Optimized structure of MNP/TC2.

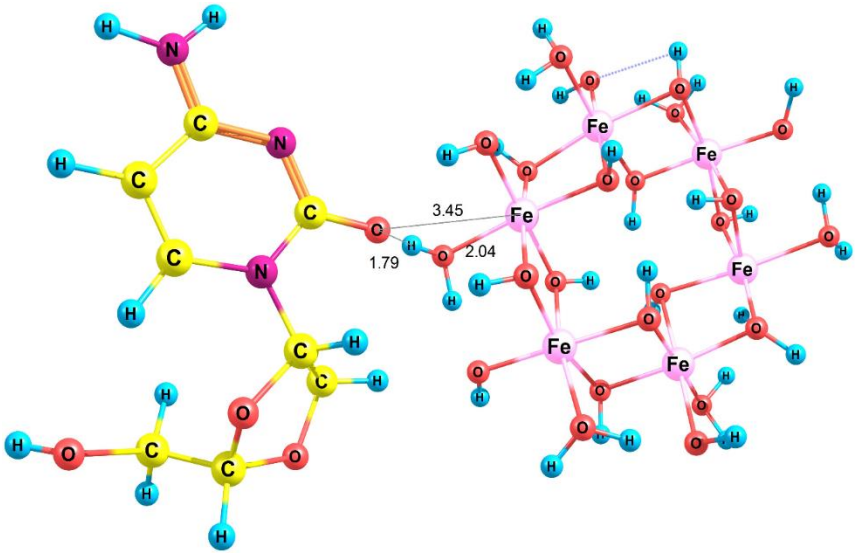

Fig. 4. Optimized structure of MNP/TC3.

Covalent functionalization

First, we considered MNP/TC1-2 configurations for the investigation of covalent functionalization in solution phase. In these cases, hydroxyl and amino groups in MNP/TC1-2 attack the Fe atom to transfer its proton to surface OH group of MNP. Scheme 1 shows the mechanism for the formation of covalent bond between TC and MNP. In these mechanisms, reactants MNP/TC1-2 are converted into the products MNPTC1-2/H_2O by losing H_2O.

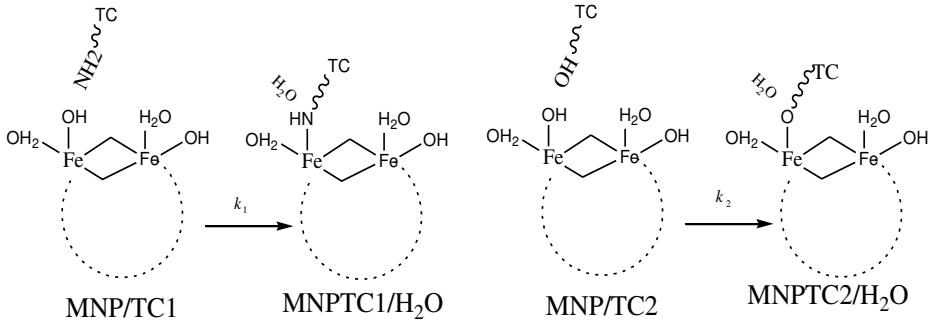

Scheme 1. k_1 and k_2 mechanisms.

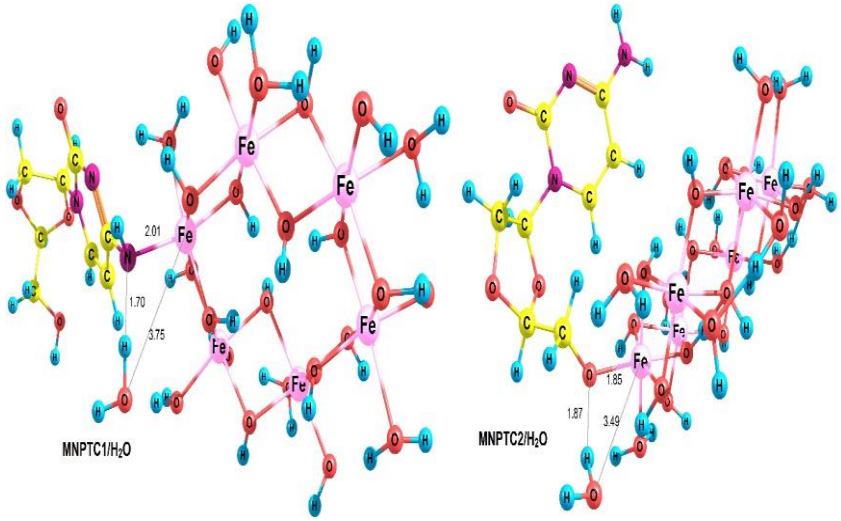

Fig. 5. Optimized structures of MNPTC1/H_2O and MNPTC2/H_2O.

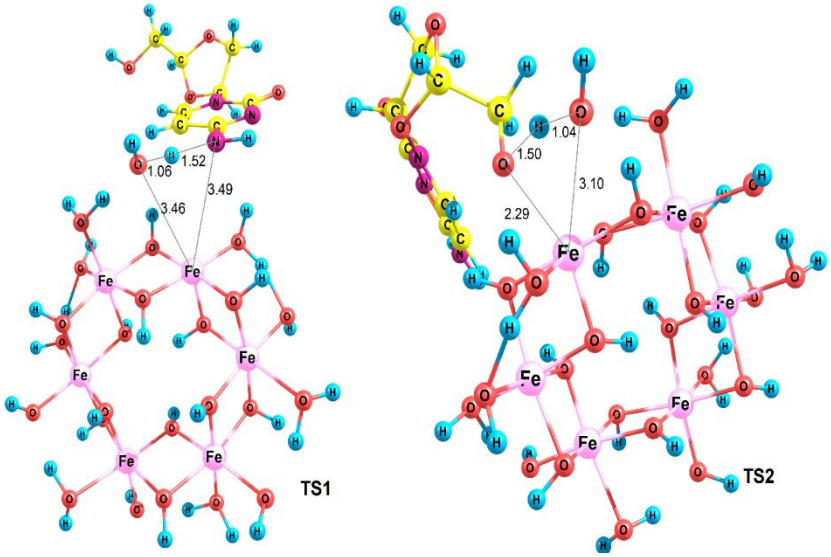

Fig. 6. Optimized structures of TS_{k1} and TS_{k2}.

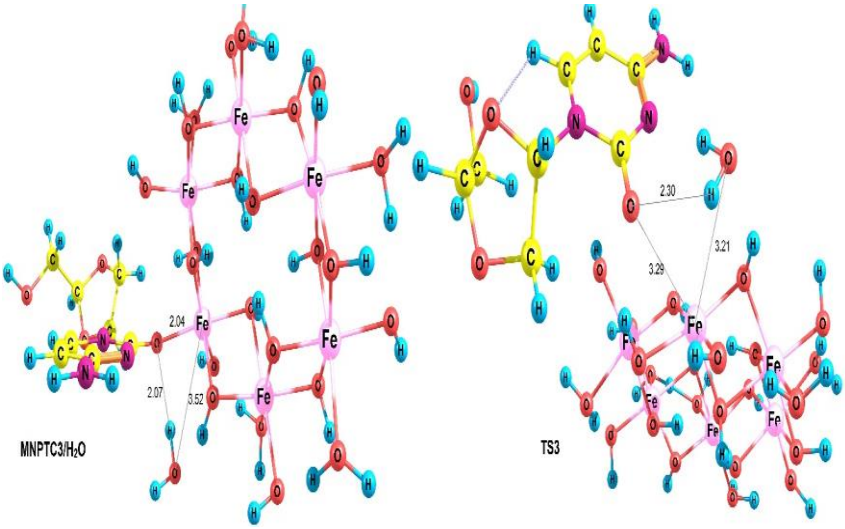

Fig. 7. Optimized structures of MNPTC3/H_2O and TS_{k3}.

According to the Scheme 1, in these mechanisms surface OH group from $Fe_6(OH)_{18}(H_2O)_6$ is substituted by NH (O) from drug TC to give product MNPTC1(2)/H_2O. The optimized structures of products MNPTC1-2/H_2O have been shown in Fig. 5. Using reactant MNP/TC1 and product MNPTC1/H_2O, the transition state of k_1 step was optimized which we call TS_{k1} (Fig. 6). The calculated bond lengths for all mechanisms have been shown in Figs. 2, 5 and 6. Relative energies for optimized structures in all pathways have been calculated in Table 3 by considering electronic plus zero-point energy (*E*), enthalpy (*H*) and Gibbs free energy (*G*) of reactants equal to zero. The activation energy (E_a), activation enthalpy ($\Delta H^{\ddagger}$) and activation Gibbs free energy ($\Delta G^{\ddagger}$) for k_1 mechanism are 117.83kJ mol^{-1}, 118.03 kJ mol^{-1}, and 128.52 kJ mol^{-1}, respectively (Table 3). Similar to k_1 step, using MNP/TC2 and MNPTC2/H_2O, the transition state of k_2 step (Fig. 6) was obtained which we call TS_{k2}. E_a, $\Delta H^{\ddagger}$ and $\Delta G^{\ddagger}$ for k_2 step are 131.80 kJ mol^{-1}, 133.34 kJ mol^{-1}, and 142.30 kJ mol^{-1}, respectively (Table 3).

The other reaction for the covalent functionalization of TC onto MNT is shown in Scheme 2. In this mechanism, H_2O from $Fe_6(OH)_{18}(H2O)_6$ is substituted by C=O group from TC to give product MNPTC3/H_2O. The optimized structures of product MNPTC3/H_2O has been shown in Fig. 7.

Table 3. Relative energies (kJ mol-1) for different species in k1-k3 mechanisms.

species	ΔE	ΔH	ΔG
		k_1 mechanism	
MNP/TC1	0.00	0.00	0.00
TS_{k1}	117.83	118.03	128.52
MNPTC1/H_2O	18.94	16.95	26.51
		k_2 mehanism	
MNP/TC2	0.00	0.00	0.00
TS_{k2}	131.80	133.34	142.30
MNPTC2/H_2O	-6.69	-9.58	-4.70
		k_3 mehanism	

MNP/TC3	0.00	0.00	0.00
TS_{k3}	84.51	86.06	92.88
MNPTC3/H_2O	38.96	39.09	41.88

Using MNP/TC3 and MNPTC3/H2O, the transition state of k_3 step (Fig. 7) was obtained which we call TS_{k3}. E_a, $\Delta H^{\ddagger}$ and $\Delta G^{\ddagger}$ for k_3 step are 84.51 kJ mol^{-1}, 86.06 kJ mol^{-1} and 92.88 kJ mol^{-1} (Table 3).

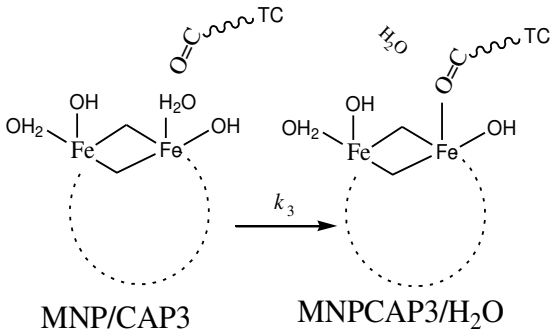

Scheme 2. k3 Mechanism.

The activation energy for k_3 mechanism is lower than k_1 and k_2 mechanisms by 33.31 kJ mol^{-1} and 47.29 kJ mol^{-1}, respectively. On the other hand, using absolute energies, product MNPTC2/H_2O (k_2 mechanisms) is more stable than products MNPTC1/H_2O (k_1 mechanisms) and MNPTC3/H_2O (k_3 mechanism) by 52.46 kJ mol^{-1} and 20.62 kJ mol^{-1}, respectively, so products MNPTC2/H_2O (high activation energies) and MNPTC3/H_2O (low activation energies) are thermodynamic and kinetic products, respectively.

In other words, thermodynamic and kinetic controls act opposite each other. The high energy barriers of k_1 and k_2 mechanisms are related to the proton transfer from OH and NH_2 of drug to OH of the cluster. Different techniques such as using ultrasonic irradiation, helps to increase the contribution of k_1 and k_2 mechanisms and is in favor of thermodynamic control.

Conclusion

Three configurations of noncovalent interaction of drug troxacitabine (TC) onto γ-Fe_2O_3 nanoparticles (MNP) were investigated in gas and solution phases. MNPs were modeled using $Fe_6(OH)_{18}(H2O)_6$ ring clusters. The binding energies for two configurations in gas and solution phases are negative, so these interactions are energetically favorable. The global hardness and HOMO-LUMO energy gap of TC are higher than MNP/TC1-3, showing the reactivity of the TC increases in the presence of γ-Fe_2O_3 nanoparticles.

Three mechanisms of covalent functionalization of drug TC onto MNP thorough NH_2 (k_1 mechanism), OH (k_2 mechanism) and C=O (k_3 mechanism) groups have been studied in detail. The activation parameters related to k_1 and k_2 mechanisms are higher than k_3 mechanism. The product of k_2 mechanism is more stable, but the product of k_3 mechanism is formed faster and therefore MNPTC3/H_2O is kinetic product.

Acknowledgements

We thank the Research Center for Animal Development Applied Biology for allocation of computer time.

References

1. Lu, A. H.; Salabas, E. e. L.; Schüth, F. Magnetic nanoparticles: synthesis, protection, functionalization, and application. Angewandte Chemie International Edition 2007, 46, 1222-1244.
2. Jun, Y.-w.; Seo, J.-w.; Cheon, J. Nanoscaling laws of magnetic nanoparticles and their applicabilities in biomedical sciences. Accounts of Chemical Research 2008, 41, 179-189.
3. Lee, S.-H.; Cha, J.; Sim, K.; Lee, J.-K. Efficient removal of arsenic using magnetic multi-granule nanoclusters. Bulletin of the Korean Chemical Society 2014, 35, 605-609.
4. Goll, D. Magnetism of nanostructured materials for advanced magnetic recording. International Journal of Materials Research 2009, 100, 652-662.
5. Sadri, F.; Ramazani, A.; Massoudi, A.; Khoobi, M.; Azizkhani, V.; Tarasi, R.; Dolatyari, L.; Min, B.-K. Magnetic CoFe2O4 nanoparticles as an efficient catalyst for the oxidation of alcohols to carbonyl compounds in the presence of oxone as an oxidant. Bull. Korean Chem. Soc 2014, 35, 2029.
6. Dua, P.; Chaudhari, K. N.; Lee, C. H.; Chaudhari, N. K.; Hong, S. W.; Yu, J.-S.; Kim, S.; Lee, D.-k. Evaluation of toxicity and gene expression changes triggered by oxide nanoparticles. Bulletin of the Korean Chemical Society 2011, 32, 2051-2057.
7. Pankhurst, Q. A.; Connolly, J.; Jones, S. K.; Dobson, J. Applications of magnetic nanoparticles in biomedicine. Journal of Physics D: Applied Physics 2003, 36, R167.
8. Berry, C. C.; Curtis, A. S. Functionalisation of magnetic nanoparticles for applications in biomedicine. Journal of Physics D: Applied Physics 2003, 36, R198.
9. Arruebo, M.; Fernández-Pacheco, R.; Ibarra, M. R.; Santamaría, J. Magnetic nanoparticles for drug delivery. Nano Today 2007, 2, 22-32.
10. Akbarzadeh, A.; Samiei, M.; Davaran, S. Magnetic nanoparticles: preparation, physical properties, and applications in biomedicine. Nanoscale research letters 2012, 7, 144.
11. Fang, C.; Zhang, M. Multifunctional magnetic nanoparticles for medical imaging applications. Journal of Materials Chemistry 2009, 19, 6258-6266.
12. Ding, G.-b.; Liu, H.-y.; Wang, Y.; Lü, Y.-y.; Wu, Y.; Guo, Y.; Xu, L. Fabrication of a magnetite nanoparticle-loaded polymeric nanoplatform for magnetically guided drug delivery. Chemical Research in Chinese Universities 2013, 29, 103-109.
13. Xu, J.; Ju, C.; Sheng, J.; Wang, F.; Zhang, Q.; Sun, G.; Sun, M. Synthesis and characterization of magnetic nanoparticles and its application in lipase immobilization. Bulletin of the Korean Chemical Society 2013, 34, 2408-2412.
14. Zhao, S. Y.; Lee, D.-G.; Kim, C.-W.; Cha, H.-G.; Kim, Y.-H.; Kang, Y.-S. Synthesis of magnetic nanoparticles of Fe 3 O 4 and CoFe 2 O 4 and their surface modification by surfactant adsorption. Bulletin of the Korean Chemical Society 2006, 27, 237-242.
15. Pennock, G. D.; Dalton, W. S.; Roeske, W. R.; Appleton, C. P.; Mosley, K.; Plezia, P.; Miller, T. P.; Salmon, S. E. Systemic toxic effects associated with high-dose verapamil infusion and chemotherapy administration. Journal of the National Cancer Institute 1991, 83, 105-110.
16. Lindley, C.; McCune, J. S.; Thomason, T. E.; Lauder, D.; Sauls, A.; Adkins, S.; Sawyer, W. T. Perception of chemotherapy side effects cancer versus noncancer patients. Cancer practice 1999, 7, 59-65.
17. Mornet, S.; Vasseur, S.; Grasset, F.; Duguet, E. Magnetic nanoparticle design for medical diagnosis and therapy. Journal of Materials Chemistry 2004, 14, 2161-2175.
18. Ito, A.; Shinkai, M.; Honda, H.; Kobayashi, T. Medical application of functionalized magnetic nanoparticles. Journal of bioscience and bioengineering 2005, 100, 1-11.
19. Dobson, J. Magnetic nanoparticles for drug delivery. Drug Development Research 2006, 67, 55-60.

20. Namdeo, M.; Saxena, S.; Tankhiwale, R.; Bajpai, M.; Mohan, Y.; Bajpai, S. Magnetic nanoparticles for drug delivery applications. Journal of Nanoscience and Nanotechnology 2008, 8, 3247-3271.
21. Morais, P.; Garg, V.; Oliveira, A.; Silveira, L.; Santos, J.; Rodrigues, M.; Tedesco, A. In ISIAME 2008; Springer: 2009, p 269-275.
22. Hua, M.-Y.; Liu, H.-L.; Yang, H.-W.; Chen, P.-Y.; Tsai, R.-Y.; Huang, C.-Y.; Tseng, I.-C.; Lyu, L.-A.; Ma, C.-C.; Tang, H.-J. The effectiveness of a magnetic nanoparticle-based delivery system for BCNU in the treatment of gliomas. Biomaterials 2011, 32, 516-527.
23. Kempe, H.; Kempe, M. The use of magnetite nanoparticles for implant-assisted magnetic drug targeting in thrombolytic therapy. Biomaterials 2010, 31, 9499-9510.
24. Vose, J. M.; Panwalkar, A.; Belanger, R.; Coiffier, B.; Baccarani, M.; Gregory, S. A.; Facon, T.; Fanin, R.; Caballero, D.; Ben-Yehuda, D. A phase II multicenter study of troxacitabine in relapsed or refractory lymphoproliferative neoplasms or multiple myeloma. Leukemia & lymphoma 2007, 48, 39-45.
25. Giles, F. J.; Cortes, J. E.; Baker, S. D.; Thomas, D. A.; O'brien, S.; Smith, T. L.; Beran, M.; Bivins, C.; Jolivet, J.; Kantarjian, H. M. Troxacitabine, a novel dioxolane nucleoside analog, has activity in patients with advanced leukemia. Journal of clinical oncology 2001, 19, 762-771.
26. Zheng, Y. B.; Kiraly, B.; Huang, T. J. Molecular machines drive smart drug delivery. Nanomedicine 2010, 5, 1309-1312.
27. Linko, V.; Ora, A.; Kostiainen, M. A. DNA nanostructures as smart drug-delivery vehicles and molecular devices. Trends in Biotechnology 2015, 33, 586-594.
28. Szymański, W.; Beierle, J. M.; Kistemaker, H. A.; Velema, W. A.; Feringa, B. L. Reversible photocontrol of biological systems by the incorporation of molecular photoswitches. Chemical Reviews 2013, 113, 6114-6178.
29. Becke, A. D. Density-functional exchange-energy approximation with correct asymptotic behavior. Physical Review A 1988, 38, 3098.
30. Becke, A. D. Density-functional thermochemistry. III. The role of exact exchange. The Journal of Chemical Physics 1993, 98, 5648-5652.
31. Lee, C.; Yang, W.; Parr, R. G. Development of the Colle-Salvetti correlation-energy formula into a functional of the electron density. Physical Review B 1988, 37, 785.
32. Frisch, M.; Trucks, G.; Schlegel, H.; Scuseria, G.; Robb, M.; Cheeseman, J.; Scalmani, G.; Barone, V.; Mennucci, B.; Petersson, G. G09 Gaussian Inc. Wallingford, CT 2009.
33. Hooman Vahidi, S.; Morsali, A.; Ali Beyramabadi, S. Quantum mechanical study on the mechanism and kinetics of the hydrolysis of organopalladium Complex [Pd (CNN) P (OMe)< sub> 3</sub>]< sup>+</sup> in low acidity range. Computational and Theoretical Chemistry 2012, 994, 41-46.
34. Akbari, A.; Hoseinzade, F.; Morsali, A.; Ali Beyramabadi, S. Quantum mechanical study on the mechanism and kinetics of the< i> cis</i>-to-< i> trans</i> isomerization of [Pd (C< sub> 6</sub> Cl< sub> 2</sub> F< sub> 3</sub>) I (PH< sub> 3</sub>)< sub> 2</sub>]. Inorganica Chimica Acta 2013, 394, 423-429.
35. Morsali, A.; Hoseinzade, F.; Akbari, A.; Beyramabadi, S. A.; Ghiasi, R. Theoretical Study of Solvent Effects on the Cis-to-Trans Isomerization of [Pd (C6Cl2F3) I (PH3) 2]. Journal of Solution Chemistry 2013, 42, 1902-1911.
36. Mohseni, S.; Bakavoli, M.; Morsali, A. Theoretical and experimental studies on the regioselectivity of epoxide ring opening by nucleophiles in nitromethane without any catalyst: nucleophilic-chain attack mechanism. Progress in Reaction Kinetics and Mechanism 2014, 39, 89-102.
37. Beyramabadi, S. A.; Eshtiagh-Hosseini, H.; Housaindokht, M. R.; Morsali, A. Mechanism and kinetics of the Wacker process: a quantum mechanical approach. Organometallics 2007, 27, 72-79.
38. Gharib, A.; Morsali, A.; Beyramabadi, S.; Chegini, H.; Ardabili, M. N. Quantum mechanical study on the rate determining steps of the reaction between 2-aminopyrimidine with dichloro-[1-methyl-2-(naphthylazo) imidazole] palladium (II) complex. Progress in Reaction Kinetics and Mechanism 2014, 39, 354-364.
39. Morsali, A. Mechanism of the Formation of Palladium (II) Maleate Complex: A DFT Approach. International Journal of Chemical Kinetics 2015, 47, 73-81.
40. Ardabili, M. N.; Morsali, A.; Beyramabadi, S. A.; Chegini, H.; Gharib, A. Quantum mechanical study of the alkoxide-independent pathway of reductive elimination of C–O from palladium (p-cyanophenyl) neopentoxide complex. Research on Chemical Intermediates 2015, 41, 5389-5398.
41. Cammi, R.; Tomasi, J. Remarks on the use of the apparent surface charges (ASC) methods in solvation problems: Iterative versus matrix-inversion procedures and the renormalization of the apparent charges. Journal of Computational Chemistry 1995, 16, 1449-1458.
42. Tomasi, J.; Persico, M. Molecular interactions in solution: an overview of methods based on continuous distributions of the solvent. Chemical Reviews 1994, 94, 2027-2094.
43. Jayarathne, L.; Ng, W.; Bandara, A.; Vitanage, M.; Dissanayake, C.; Weerasooriya, R. Fabrication of succinic acid-γ-Fe_2O_3 nano core–shells. Colloids and surfaces 2012.
44. Parr, R. G.; Szentpaly, L. v.; Liu, S. Electrophilicity index. Journal of the American Chemical Society 1999, 121, 1922-1924.